Impact of Phosphorylation on the Physiological Form of Human alpha-Synuclein in Aqueous Solution

Emile de Bruyn,[†,‡,¶] Anton Emil Dorn,[†,‡,§] Giulia Rossetti,[*,‡,‖,⊥] Claudio Fernandez,[#,@] Tiago F. Outeiro,[△,∇,††] Jörg B. Schulz,[¶,⊥,‡‡] and Paolo Carloni[¶,‖]

† *Equally contributed to this work*
‡ *Jülich Supercomputing Centre (JSC), Forschungszentrum Jülich GmbH, 52425 Jülich, Germany*
¶ *Department of Physics, RWTH Aachen University, 52062 Aachen, Germany*
§ *Faculty of Biology, University of Duisburg-Essen, 45141 Essen, Germany*
‖ *Computational Biomedicine (IAS-5/INM-9), Forschungszentrum Jülich GmbH, 52425 Jülich, Germany*
⊥ *Department of Neurology, RWTH Aachen University, 52074 Aachen, Germany*
Max Planck Laboratory for Structural Biology, Chemistry and Molecular Biophysics of Rosario (MPLbioR, UNR-MPINAT). Partner of the Max Planck Institute for Multidisciplinary Sciences (MPINAT, MPG). Centro de Estudios Interdisciplinarios, Universidad Nacional de Rosario, S2002LRK Rosario, Argentina
@ *Department of NMR-based Structural Biology, Max Planck Institute for Multidisciplinary Sciences, 37077 Göttingen, Germany*
△ *Department of Experimental Neurodegeneration, Center for Biostructural Imaging of Neurodegeneration, University Medical Center Göttingen, 37075 Göttingen, Germany*
∇ *Max Planck Institute for Multidisciplinary Sciences, 37075 Göttingen, Germany*
†† *Translational and Clinical Research Institute, Newcastle University, Newcastle upon Tyne NE1 7RU, United Kingdom*
‡‡ *JARA Brain Institute Molecular Neuroscience and Neuroimaging (INM-11), Research Centre Jülich and RWTH Aachen University, 52074 Aachen, Germany*

E-mail: g.rossetti@fz-juelich.de

Abstract

Serine 129 can be phosphorylated in pathological inclusions formed by the intrinsically disordered protein human α-synuclein (AS), a key player in Parkinson's disease and other synucleinopathies. Here, molecular simulations provide insight into the structural ensemble of phosphorylated AS. The simulations allow us to suggest that

phosphorylation does significantly impact the structural content of the physiological AS conformational ensemble in aqueous solution, as the phosphate group is mostly solvated. The hydrophobic region of AS contains β-hairpin structures, which may increase the propensity of the protein to undergo amyloid formation, as seen in the non-physiological (non-acetylated) form of the protein in a recent molecular simulation study. Our findings are consistent with existing experimental data, with the caveat of the observed limitations of the force field for the phosphorylated moiety.

Introduction

Parkinson's disease (PD) is the second most common neurodegenerative disease after Alzheimer's disease,[1] affecting several million people worldwide.[2,3] The typical pathological hallmark is the accumulation of fibrillar protein inclusions, know as Lewy bodies (LBs) and Lewy neurites (LNs) in the brain.[4,5] The major component of LBs and LNs are fibrillar forms of the human α-synuclein (AS) protein.[3,6] AS is a 140 amino acid *disordered* conformational ensemble both in aqueous solution and in vivo. AS acquires some degree of structure when bound to the membrane or to cellular partners.[7,8]

The primary sequence of AS can be divided in three domains: the positively charged N-terminus (residues 1-60), the overall neutral hydrophobic region (residues 61-95)[1] and the negatively charged C-terminal domain (residues 96-140, Figure 1). Under physiological conditions, the protein is acetylated on the first residue[2] In LBs, a significant fraction of AS is phosphorylated on S129.[3,11] S129 phosphorylation may be regulated by neuronal activity, suggesting that the process may be part of the normal physiology of AS.[12,13] This post-translational modification (PTM) might play also a pathological role.[14–17] S129 phosphorylation may be regulated by neuronal activity, suggesting that the process may be part

[1] We choose to use the more accurate term "hydrophobic region" instead of the historical but inaccurate term "non-amyloid component (NAC)".[9]

[2] N-terminal acetylation does not significantly change the fibrillization propensity in vitro.[10]

[3] Another phosphorylation site of α-synuclein at T64 has also been described.[10]

of the normal physiology of AS.[12,13]

```
MDVFMKGLSKAKEGVVAAAEKTKQGVAEAAGKTKE  35
GVLYVGSKTKEGVVHGVATVAEKTKEQVTNVGGAV  70
VTGVTAVAQKTVEGAGSIAAATGFVKKDQLGKNEE 105
GAPQEGILEDMPVDPDNEAYEMPSEEGYQDYEPEA 140
```

Figure 1: Sequence of amino acid residues in AS; positively charged residues are highlighted in blue and negatively charged ones in red. Three domains can be identified: the positively charged N-terminus (residues 1-60), the overall neutral hydrophobic region (residues 61-95) and the negatively charged C-terminal domain (residues 96-104). In physiological conditions, the protein is acetylated on the first residue, although this post-translational modification does not significantly affect the fibrillization propensity in vitro.[18] In LBs, a significant fraction of AS is phosphorylated on S129.[11] A novel phosphorylation site at T64 has also been recently described.[10]

The formation of the S129-O-PO_3^{2-} group at the C-terminus of phosphorylated α synuclein (pAS) instead of one of the other two domains is intriguing, because it introduces as many as two negative charges at physiological pH (the pKa_1 and pKa_2 of phosphoserine are < 2 and 5.6[19]).[4]

The impact of phosphorylation on the structural ensemble and aggregation propensity of physiological AS is not known. Thus far, Circular Dichroisim (CD) studies on the non-N-term acetylated form of the protein in solution show that the conformational ensemble does not change significantly upon S129 phosphorylation.[20,21] [5] On the detailed molecular level, replica exchange simulations based on the CHARMM36m force field[23] point to an increase of looped secondary structure close to a β-hairpin spread throughout the hydrophobic region upon phosphorylation.[24] However, the structure of the physiological form differs from that of the non-acetylated one (which does not exist in human cells),[25–27] so firm conclusions on the effect of phosphorylation on endogenous AS cannot be made from these studies.

Here we investigate the impact of phosphorylation on the physiological form of AS by molecular simulation. For this study, one may face several challenges. First, the force

[4]It might be possible that the phosphate is partially monoprotonated. The effect of protonation is discussed in the Supplementary Information.

[5]This contrasts with findings by CD studies for phosphorylation on protein variants.[20–22] These point to significant changes in the structural ensemble upon phosphorylation.

field must be adequate to describe IDPs such as AS. The DES-Amber ff99SB,[28] the Amber a99SB-*disp*[29] and CHARMM36m[23] force fields have been tailored for IDPs;[29–31] the last two have been successfully used for the non-acetylated form of the proteins.[29,31,32] All of these force fields appear therefore to be well suited to study AS. Second, accurately describing a doubly charged group such as phosphate in pAS is non-trivial. Indeed, Amber[33–35] and CHARMM[36,37] based simulations of phosphorylated protein have at times shown artifacts.[38–41] Therefore, we have adapted phosphate parameters from the DES-AMBER DNA force field,[42] recently calibrated on osmotic coefficient calculations. Finally, the conformational space of the protein structural ensemble needs to be efficiently explored. Among the many methodologies used to investigate IDPs successfully,[43–52] our predictions based on Replica Exchange with Solute Tempering 2 (REST2)[53] enhanced sampling predictions of wild-type[54,55] and mutants of AS,[55,56] turned out to reproduce a variety of biophysical properties of the protein and hence they appear well suitable to study this problem.

Here, we present 600 ns REST2 simulations of AS and pAS based on the DES-Amber[42] and a99SB-*disp* force-fields.[29] We use TIP4P-D for DES-Amber, and the accompanying modified TIP4P-D water model for a99SB-*disp*. To the best of the authors' knowledge, these simulations are the only ones so far (i) reporting on the physiological form of AS in explicit solvent,[6] and (ii) describing in detail the hydration properties of the phosphate, which has never been reported in previous simulation studies.[38–41,81–85]

Methods

Molecular Simulations

System. The structure of the acetylated protein (AS) which best reproduced the chemical shifts in ref. 86 was selected from the conformational ensemble previously reported in ref.

[6]Many molecular simulation studies, besides those in refs. 29 and 32, focus on the non-acetylated protein.[31,57–59,59–80] Calculations of the protein in implicit solvent are not reported here.

54. The phosphorylated protein (pAS) was built by adding a phosphate group to S129 using PyMOL.[87]

AS and pAS were inserted in a water-filled dodecahedral simulation box with periodic boundary conditions and minimum distance of 35 Å between the protein and the box edges. Na^+ and Cl^- ions were added to neutralize the system and achieve a concentration of 150 mmol L^{-1}. Table 1 shows the composition of the systems.

Table 1: Number of atoms of the systems simulated here.

	Protein	Water	Sodium	Chlorine
AS	2,020	190,533	186	176
pAS	2,023	172,359	171	159

Force fields. The simulations were based on: (i) the DES-Amber force field[28] and the standard TIP4P-D water model[88] (Table S1 for a full list of the parameters used); (ii) the a99SB-*disp* force field[29] and its accompanying modified TIP4P-D water model.[29]

Molecular simulation setup. Long range electrostatics were evaluated using the Particle-Mesh Ewald (PME) method,[89] using a cutoff distance of 12 Å in real space. The van der Waals interactions featured the same cutoff. Constant temperature conditions were achieved by coupling the systems with a Nosé-Hoover thermostat[90] at 300 K, with a time constant of 0.5 ps. Constant pressure was achieved with a Parrinello-Rahman barostat[91] at 1 bar, with a time constant of 2 ps (Table S1). The LINCS algorithm was used for all bonds involving hydrogen atoms.[92] The equations of motions were integrated using the `md` leap-frog algorithm, with a timestep of 2 fs.

MD and REST simulations. The proteins underwent energy minimization (Table S2), and, subsequently 100 ps of MD in the NVT ensemble (Table S3). Then, they were heated up in 25 ps-long steps of 5 K in the same ensemble up to 300 K using simulated annealing (Tables S4 and S5). The systems were further equilibrated for 1 ns in the NPT ensemble (Table S6). Finally, they underwent 600 ns REST2 simulations[53] in the NPT ensemble, with a total of 32 replicas between 300 and 500 K exchanging every 1.000 simulation steps. The

proteins were not found to be near their periodic images at distances lower than 12 Å during any of these simulations. The simulations converged after 100 ns (see the Results Section).

Structurally similar conformational clusters were obtained following the method for clustering IDPs described in ref. 93: For both AS and pAS, a total of 5.000 frames from the last 500 ns were clustered (Figures S7 and S8).

Calculated properties. Based on the last 500 ns REST simulations, we obtained representative structures were obtained (using the method for clustering IDPs in ref. 93, Figures S7 and S8), and we calculated the following properties: (i) The radius of gyration R_g, calculated using the MDTraj Python code.[94] (ii) The hydrodynamic radius, calculated from the radii of gyration using the linear fit of ref. 67. (iii) The protein end-to-end distance between the N- and C-termini, using the MDTraj Python code.[94] (iv) The NMR chemical shifts of backbone nitrogen, hydrogen, C_α, C_β and backbone carbonyl carbon atoms, using the SPARTA+ code.[95] (v) The CD spectra of representative cluster structures, using the SESCA code.[96–98] (vi) The solvent accessible surface area (SASA) using the MDTraj code.[94] (vii) The contact map of protein residues using minimum pairwise distances between residues using the MDTraj code.[94] (viii) Radial distribution functions (RDFs) and time-resolved radial distribution functions (TRRDFs) using the SPEADI[99,100] code developed by the authors.

(ix) Hydrogen bonds were defined according to the scheme in ref. 101. (x) Salt bridges were defined using a distance between two charged atoms in the protein at a distance below 3.25 Å as in ref. 102. (xi) Secondary structure elements were identified using MDTraj[94] and DSSP.[103] (xii) Free energy profiles (or potentials of mean force, PMFs) were calculated according to ref. 104 by constructing a 2-dimensional histogram of the radius of gyration and end-to-end distance of the protein along the converged part of the simulation, and subsequently performing a Boltzmann inversion of the histogram:

$$\Delta G_i = -k_\mathrm{B} T \ln\left(\frac{\rho_i}{\rho_\mathrm{min}}\right), \tag{1}$$

where ΔG_i is the free energy at a point relative to the least dense part of the surface, and ρ_i is the density at that point.

Validation of the REST2 setup. To investigate the impact of our REST2 setup parameters on our results, we performed additional 60 ns simulations with higher replicas (64) and temperatures ranging between 300 and 600 K. Comparison with 60 ns with our setup (32 replicas and temperatures ranging from 300 and 500 K) shows that these new simulations explore less efficiently the protein conformational space. Thus, increasing the number of replicas and maximum temperature does not lead to an improvement of the results. A rationale for this result is provided in the SI at p. 42 and with Figures S1 and S2.

Results and Discussion

We performed REST2 simulations[53] for 600 ns, using 32 replicas, for both AS and pAS in aqueous solution. Figures S3 and S4 provide details on the exchange between replicas. The root mean-square deviation (RMSD) of the simulations demonstrate that the lowest temperature replica were not trapped in local minima (Figure S5). The calculations were based on the DES-Amber[42] and the a99SB-*disp* force fields,[29] both already used for IDPs. We report results at length for calculations using the former, while we provide a summary for the latter here and details in the Supplementary Information.

Convergence. We calculated two quantities as a function of simulated time to investigate the convergence of the systems (Figure S6): (i) the running averages of the percentage of secondary structures. In particular, helix structures reached a plateau after 100 ns; (ii) the running averages of the C_α chemical shifts which converge closely to the experimental values within 100 ns. Because of the limitations of the standard usage of RMSD with IDPs such as AS,[105] the running RMSD of atomic positions was not taken into account beyond monitoring the simulations. Based on this analysis, we calculated all properties in the interval

100–600 ns.

Comparison with experiment. Experimental data was compared to properties calculated from the trajectories after the determined convergence of 100 ns.

For each residue in the protein, the chemical shifts of backbone nitrogen, hydrogen, C_α, C_β, and backbone carbonyl carbon atoms were calculated where present in the structure. Comparison was made with the experimental values published in ref. 86 (Figure 2).

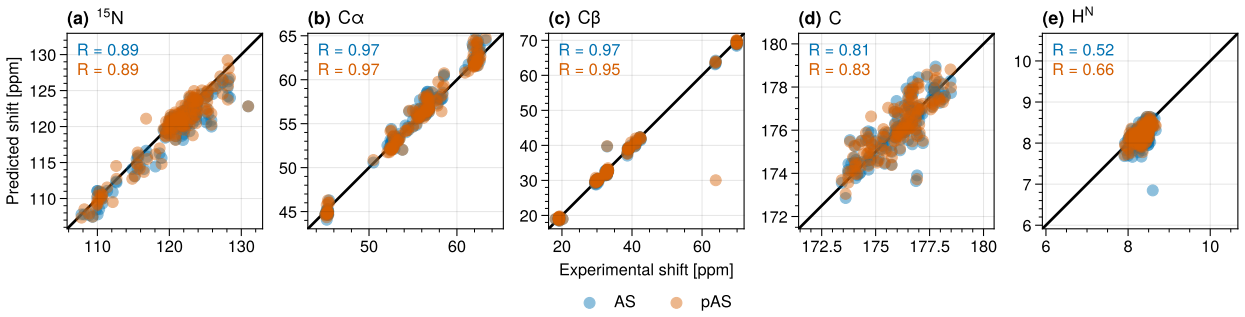

Figure 2: Calculated chemical shifts of (a) N, (b) C_α, (c) C_β, (d) C, and (e) H atoms and in AS and pAS against the experimental data from Roche et al.[86] Correlation coefficients are given for AS (blue) and pAS (orange), respectively.

The calculated chemical shifts of ^{15}N, as well as the ^{13}C-NMR chemical shifts of C_α and C_β are in excellent agreement with the experimental values, both for AS and pAS. The calculated shifts for the backbone carbonyl carbon atoms correlate less well with those obtained through experiment, yet are still broadly comparable. The calculated shifts for heavy atoms overall are in better agreement than those reported previously by some of the authors in ref. 54, possibly because a much longer exploration of the conformational ensemble has been covered here (a total of 90 ns of REST2 simulations in ref. 54 and 500 ns REST2 simulations here). The predicted shifts for ^{1}H-NMR are generally less accurate, a well known weakness of current chemical shift prediction methods,[106] and was previously observed in calculated values from MD simulations of AS in ref. 54.

The calculated CD spectra of AS and pAS are in fair accord with experimentally measured spectra[27] (Figure 3). The minima of the calculated spectra are shifted 6 nm higher than the

experimentally obtained values (204 nm and 198 nm, respectively), similar to what was found in ref. 54.

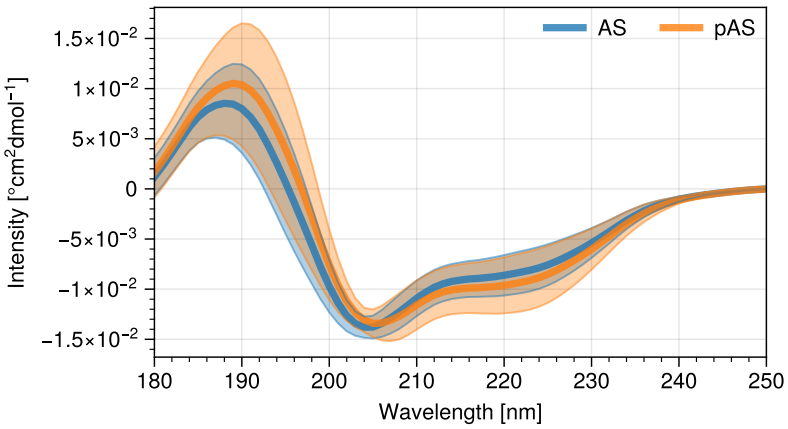

Figure 3: Circular Dichroism spectra of the AS and pAS cluster midpoint structures obtained during the converged part of the simulations. Shading indicates the standard error.

The minima of the calculated spectra range up to $-15 \cdot 10^{-3}\,^{\circ}\,\mathrm{cm}^2\,\mathrm{dmol}^{-1}$ for specific conformations, similar to what found by the authors previously. As to be expected given the improvement in force fields, these minima average to $-14 \cdot 10^{-3}\,^{\circ}\,\mathrm{cm}^2\,\mathrm{dmol}^{-1}$ for both AS and pAS, in much better agreement with the experimental results compared to previous results using the Amber ff99SB-*ildn* force field and TIP3P water model.[54] The minima in the experimental spectra of Maltsev et al. are found at $-19 \cdot 10^{-3}\,^{\circ}\,\mathrm{cm}^2\,\mathrm{dmol}^{-1}$.

Effect of phosphorylation on the protein. The AS ensemble, on average, is less compact than pAS (Figure 4). In AS, the C-terminal domain is further from the N-terminal domain, with the hydrophobic region situated between them. Phosphorylation increases the number of contacts between the C- and N-terminal domains, causing the hydrophobic region to shift to the side of the protein.

The ten largest conformational clusters of AS and pAS (from I to X in Figure 4) represent a total of 48.85 % and 49.63 % of the converged simulation trajectories, respectively (Table S7).[7]

[7]The single conformational clusters are displayed in Figures S9 and S10.

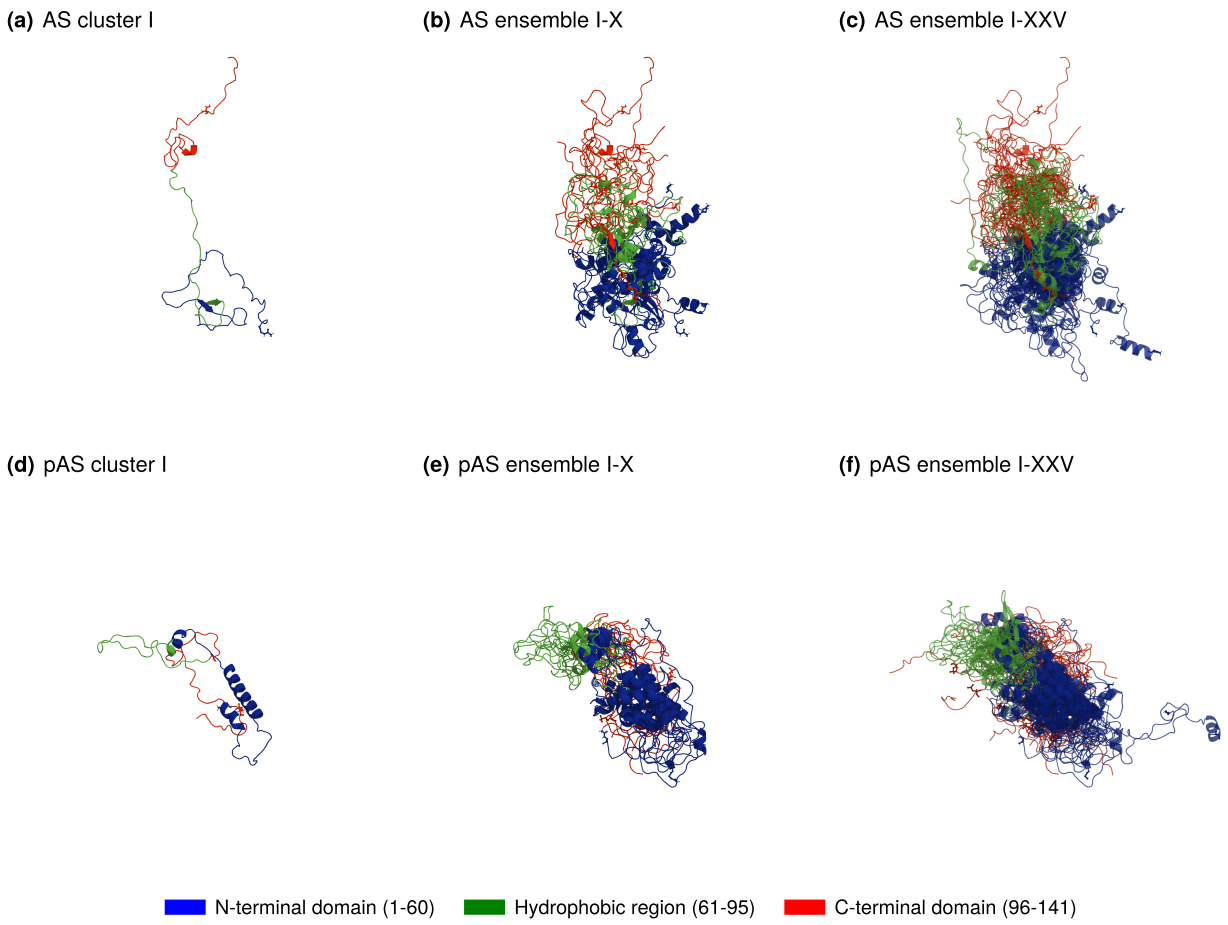

Figure 4: Structures of cluster midpoints representing the structural ensembles of AS (a-c) and pAS (d-f), from (a) 6.80 %, to (b) 48.85 %, (c) 100 %, (d) 5.80 %, (e) 49.63 %, and (f) 100 %. See Table S7 for details.

The calculated mean hydrodynamic radii (R_H) and the mean radii of gyration (R_g) decrease significantly upon phosphorylation. The distribution of R_g of AS is broader than that of pAS (Figure 5(a)). The first properties (within the standard deviation) agree with experiment (28.2 and 35.3 Å for AS and pAS,[22] respectively, Table 2).

An approximate estimate of the potential of mean force (PMF, see Methods), as a function of the radius of gyration and end-to-end distance of the protein, provides qualitative insights on the change in the free energy landscape of the protein upon phosphorylation. Figure 5(b-c) shows that the system passes from the shallow multi-basin landscape of AS (Figure 5(b)), to the bivariate-like basin distribution for pAS (Figure 5(c)). This qualitative comparison

Table 2: Calculated properties of AS and pAS with standard deviation. (i) Hydrodynamic R_H and gyration (R_g) radii of the protein. (ii) Average number of hydrogen bonds. (iii) Average number of salt bridges.

Protein	R_H [Å]	R_g [Å]	N_{SB}	N_{HB}
AS	43.9 ± 21.2	61.3 ± 15.2	3.13 ± 2.23	19.52 ± 4.28
pAS	34.0 ± 19.0	33.5 ± 12.8	3.78 ± 2.64	20.67 ± 4.32
Mean change	-9.90	-27.80	0.65	1.15

suggests that phosphorylation induces a clear cut separation between extended and compact ensembles of conformations for AS.

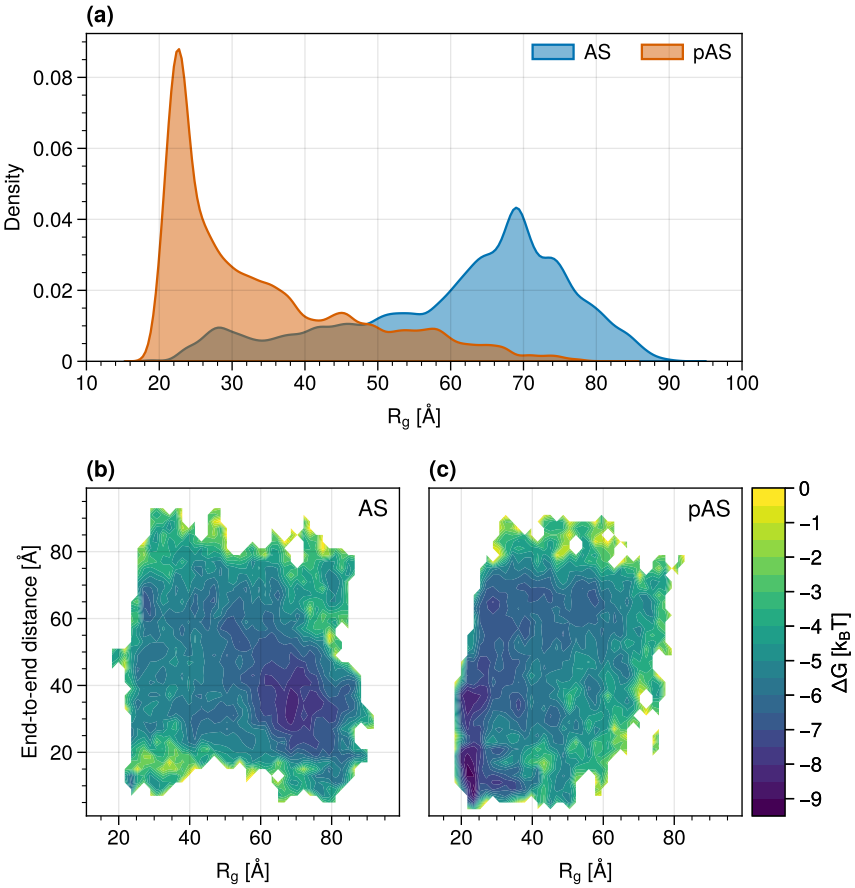

Figure 5: AS (blue) and pAS (orange) R_g distributions (a) and corresponding approximate free energy landscapes over the distance between the protein termini and radii of gyration (b-c).

The intramolecular interactions between the hydrophobic region and the C-terminus decrease upon phosphorylation; the C-terminus instead interacts with the N-terminal domain

(Figure 6). The first dozen residues interacts with the hydrophobic region, in AS, while they interact with the N-terminal region in pAS (Figure 6(b)).

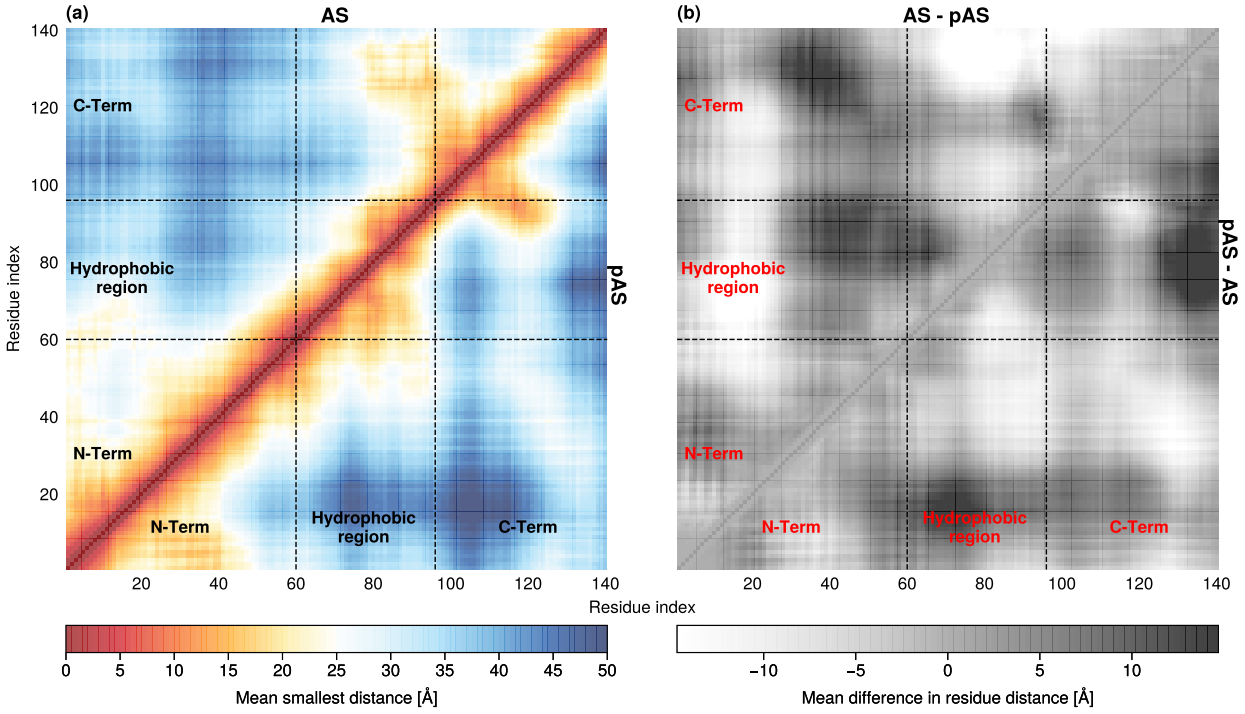

Figure 6: (a) Contact maps of AS (triangle above) and pAS (triangle below), and (b) their differences. Brighter values correspond to closer distances in the corresponding triangle compared to the opposite triangle.

The number of hydrogen bonds and salt bridges within their standard deviations do not change significantly upon phosphorylation (Figure 7, Table 2). While the first are almost exclusively formed within every single domain (Figure 7(a-b)), persistent salt bridges are formed for both proteins between the N-term and hydrophobic regions (K23–E20 and K58–E61, respectively, Figure 7(c)). Few salt bridges are formed between the C-terminal domain and one of the two other domains, such as E130–K80 in AS[8] and D135–K32 in pAS.

[8]The absence of the E130–K80 in pAS might be caused by the presence of sodium counter ions close to the pS129 residue (Figures 8 and 9).

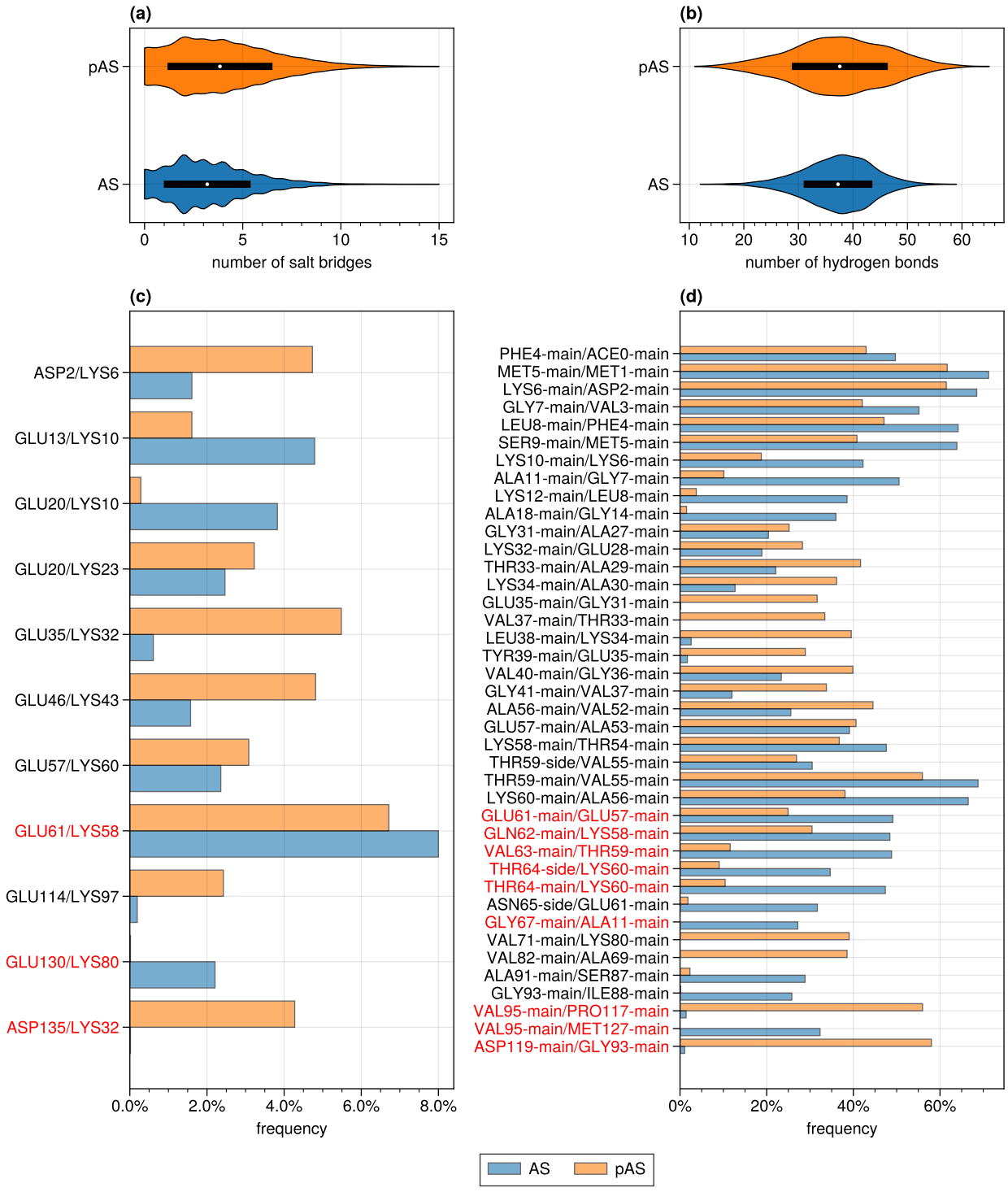

Figure 7: Distribution of the total number of salt bridges (a) and hydrogen bonds (b) in AS (blue) and pAS (orange). Frequency with which intradomain (black labels) and interdomain (red labels) salt bridges (c) and hydrogen bonds (d) are found in AS and pAS. Salt bridges and hydrogen bonds are displayed that occur during at least 2 % and 25 % of the converged trajectory, respectively, in either the AS or pAS simulation.

The Average Solvent Accessible Surface Area (SASA) decreases upon phosphorylation (Table 3). However, the decline is rather small (within the standard deviation) at the N-term and in the hydrophobic region.

Table 3: Calculated SASA in the three domains of AS and pAS.

Protein	$SASA_{N\text{-}term}$ [Å^2]	$SASA_{HydrophR}$ [Å^2]	$SASA_{C\text{-}term}$ [Å^2]
AS	6112.4 ± 603.1	3478.1 ± 585.6	6952.6 ± 762.4
pAS	5732.3 ± 726.3	3104.0 ± 472.0	6035.0 ± 955.3
Mean change	-380.1	-374.1	-917.6

Phosphate interactions. The phosphate group is fully solvent-exposed and associated with sodium counterions, without interactions with pAS residues (Figures 8 and 9). Thus, its electrostatic field is strongly reduced and its long range electrostatic interactions with the C-terminus and N-terminus are expected to be strongly screened (Figure 7).

The S129 side-chain in AS is less hydrated than in pAS: while the Oγ atom is surrounded on average by two water molecules in the first hydration shell in both AS and pAS, the second and third hydration shells contain many more water molecules in pAS (Figure 8). The serine oxydril group in AS instead forms a variety of *intramolecular* H-bonds (with K80, K96, K97, K102, E126, E130 and E131; Figure S19). S129 backbone units are observed to interact both with the solvent and nearby protein hydrogens in both AS and pAS. Thus, S129 in AS forms many more intramolecular contacts than the corresponding phosphorylated residue in pAS.

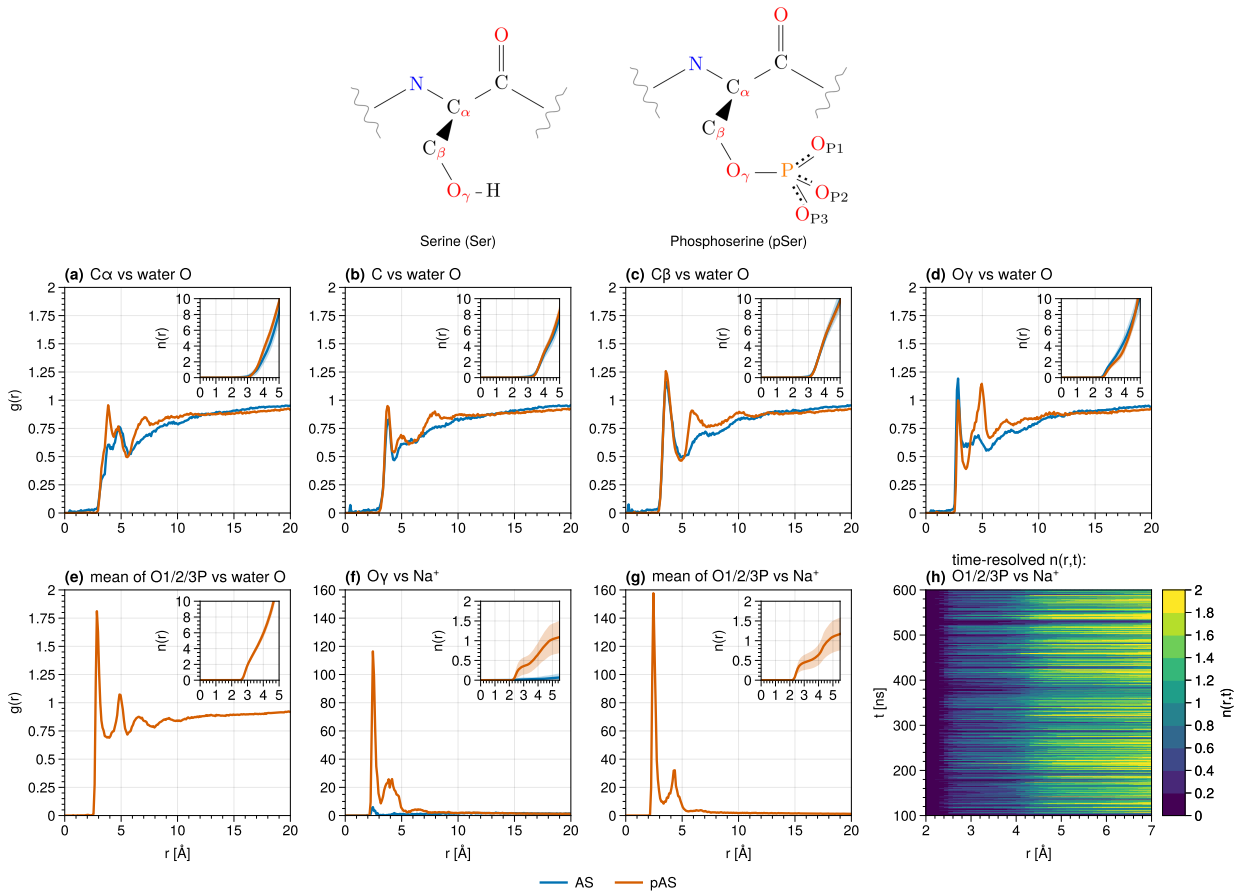

Figure 8: RDFs ($g(r)$) of (a-e) water oxygen atoms surrounding (a-b) backbone carbon atoms, (c) side-chain carbon and (d-e) side-chain oxygen atoms. (f-g) RDFs of sodium ions surrounding side-chain oxygen atoms. (h) Integral of the TRRDF ($n(r,t)$) of sodium ions over 1 ns time windows. Insets show the integral of $g(r)$ up to 5 Å.

The hydration of AS N-terminal and hydrophobic domains is comparable to that of pAS (Figure 9(a-b)). The hydration of the C-terminal domain instead increases upon phosphorylation, possibly because of the presence of the highly charged group (from 12.3 ± 3.3 water molecules surrounding S129 to 19.5 ± 2.7 around pSer129).

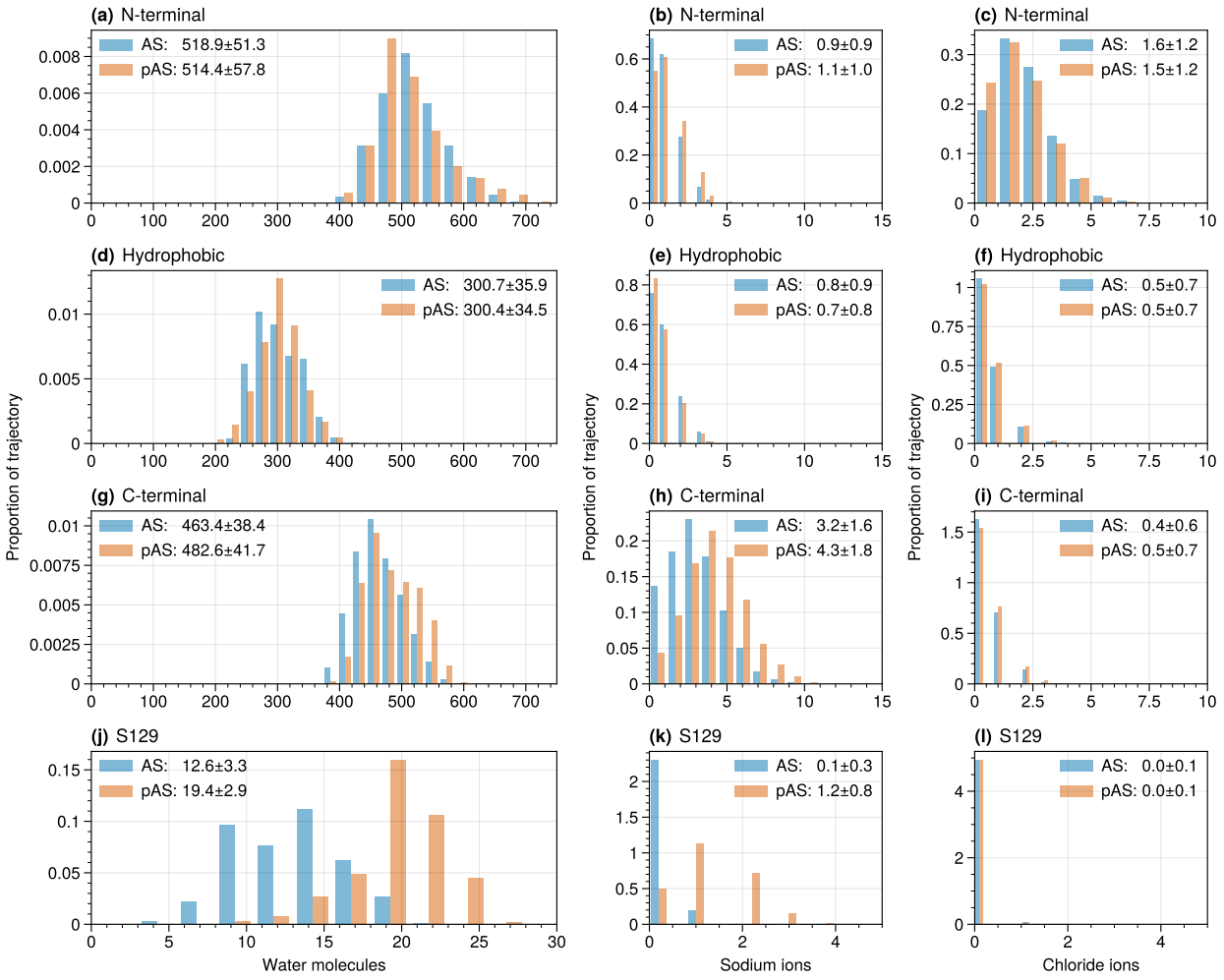

Figure 9: Number of (a,d,g,j) water molecules, (b,e,h,k) sodium ions and (c,f,i,l) chloride ions in the first hydration shell surrounding the (a-c) N-terminal, (d-f) hydrophobic, and (g-i) C-terminal domains of the protein, as well as around (j-l) the S129 residue. Inset numbers indicate the mean and standard deviation of the distributions.

Additional simulations. The simulations of AS and pAS with the Amber a99SB-*disp* force field[29] show very similar results as those presented here, except for the phosphate hydration properties, which turn out to be less accurate than those of the DES-Amber force field (See Supplementary Information, Sections 4, 5).

The simulations of the protein with monoprotonated phosphate (based on the a99SB-*disp* force field) turn out to be rather similar to those of pAS (see Supplementary Information, Section 6). Thus, we conclude that if such species exist in equilibrium with pAS, they

contribute to the protein structural ensemble similarly to pAS.

Role of phosphorylation for AS fibril formation. Our study in line with experimental studies showing that phosphorylation and de-phosphorylation of AS are likely normal physiological processes fine-tuning binding to lipids,[107,108] and they are not a clear marker of pathology.[12,13] These findings however, do strengthen the prevailing view that phosphorylation of the monomer is also implicated in fibril formation, due to the change in the structural ensemble and relative positioning of the domains. In addition, the content of β-hairpin-like structure in the hydrophobic region (calculated as in ref. 24) turns out to increase upon phosphorylation (Figure S23).[9] As discussed in ref. 24, these types of structures may be associated with amyloid-forming conformations and hence this finding does suggest that phosphorylation increases fibril formation starting from conformations similar to those found in the fibrils.[109,110] This might be consistent with the fact that almost all the proteins in the fibrils are phosphorylated *in vivo*.[11]

Conclusions

Because of the presence *in vivo* of phosphorylated AS, the detailed understanding of the impact of phosphorylation on this protein is important for informing therapeutic strategies aimed at targeting AS in synucleinopathies. Here, we investigated the effects of phosphorylation on the structural ensemble of AS in solution by 600 ns REST2 simulations based on apt force fields such as DES-Amber and Amber a99SB-*disp*. Our REST2 simulations of AS, much longer than the previously reported ones,[54] are consistent with a plethora of experimental data.The physiological form of pAS turns out to be more compact than the unmodified protein. The phosphate moiety is solvent exposed, without forming specific intramolecular interactions. The phosphorylation of the protein turns out to induce β-hairpin-like, amyloid-forming conformations. The increased propensity towards fibril formation might be

[9]This content is however smaller than that observed for the non-physiological form, see details in the Supplementary Information.

consistent with the fact that about 90 % AS in the LBs is phosphorylated.[11]

Data and Software Availability

GROMACS 2022.6 patched with PLUMED 2.9.0 was used to perform all MD simulations (`https://www.gromacs.org/` and `https://www.plumed.org/`). All analysis employing third-party software are described and referenced in the Methods section. RDFs were obtained using the authors' open-source Python package SPEADI (`https://github.com/FZJ-JSC/speadi` and `https://pypi.org/project/SPEADI/`). Charts and plots were made using the open-source Python package ProPlot (`https://github.com/proplot-dev/proplot`). Molecular structures were visualized using Open-Source PyMOL (`https://github.com/schrodinger/pymol-open-source`).

Primary data available to reproduce the study (parameterized GROMACS topologies, input files, and trajectories) are deposited in Zenodo: `https://zenodo.org/records/12605636`.

Supporting Information Available

Detailed experimental setup (including all GROMACS parameters), analysis and comparison with results obtained with other force fields are contained in the Supplementary Information (PDF).

Structures of the 25 cluster midpoints are included for both AS and pAS (PDB).

Acknowledgement

TFO is supported by DFG (SFB1286-B8) and under Germany's Excellence Strategy - EXC 2067/1- 390729940.

This work was partially performed as part of the Helmholtz School for Data Science in Life, Earth and Energy (HDS-LEE) and received funding from the Helmholtz Association of

German Research Centers.

Open Access publication funded by the Deutsche Forschungsgemeinschaft (DFG, German Research Foundation) – 491111487.

The authors gratefully acknowledge the Gauss Centre for Supercomputing e.V. (www.gauss-centre.eu) for funding this project by providing computing time through the John von Neumann Institute for Computing (NIC) on the GCS Supercomputer JUWELS at Jülich Supercomputing Centre (JSC).[111–114]

The authors gratefully acknowledge computing time on the supercomputer JURECA[115] at Forschungszentrum Jülich under grant no. 30260.

The authors gratefully acknowledge insightful discussions with Stefano Piana-Agostinetti regarding the choice of force field parameters, in particular with respect to the hydration of the phosphate group.

References

(1) Hou, Y.; Dan, X.; Babbar, M.; Wei, Y.; Hasselbalch, S. G.; Croteau, D. L.; Bohr, V. A. Ageing as a risk factor for neurodegenerative disease. *Nature Reviews Neurology* **2019**, *15*, 565–581.

(2) Rocca, W. A. The burden of Parkinson's disease: a worldwide perspective. *The Lancet* **2018**, *17*, 928–929.

(3) Lücking, C. B.; Brice, A. Alpha-synuclein and Parkinson's disease. *Cellular and Molecular Life Sciences CMLS* **2000**, *57*, 1894–1908.

(4) Baba, M.; Nakajo, S.; Tu, P.-H.; Tomita, T.; Nakaya, K.; Lee, V.; Trojanowski, J. Q.; Iwatsubo, T. Aggregation of alpha-synuclein in Lewy bodies of sporadic Parkinson's disease and dementia with Lewy bodies. *The American journal of pathology* **1998**, *152*, 879–884.

(5) Gibb, W.; Lees, A. The relevance of the Lewy body to the pathogenesis of idiopathic Parkinson's disease. *Journal of Neurology, Neurosurgery & Psychiatry* **1988**, *51*, 745–752.

(6) Nguyen, P. H.; Ramamoorthy, A.; Sahoo, B. R.; Zheng, J.; Faller, P.; Straub, J. E.; Dominguez, L.; Shea, J.-E.; Dokholyan, N. V.; De Simone, A. *et al.* Amyloid oligomers: A joint experimental/computational perspective on Alzheimer's disease, Parkinson's disease, type II diabetes, and amyotrophic lateral sclerosis. *Chemical reviews* **2021**, *121*, 2545–2647.

(7) Snead, D.; Eliezer, D. Alpha-synuclein function and dysfunction on cellular membranes. *Experimental neurobiology* **2014**, *23*, 292.

(8) Waudby, C. A.; Camilloni, C.; Fitzpatrick, A. W.; Cabrita, L. D.; Dobson, C. M.; Vendruscolo, M.; Christodoulou, J. In-cell NMR characterization of the secondary structure populations of a disordered conformation of α-synuclein within E. coli cells. *PloS one* **2013**, *8*, e72286.

(9) Goedert, M.; Griesinger, C.; Outeiro, T. F.; Riek, R.; Schröder, G. F.; Spillantini, M. G. Abandon the Nac in α-synuclein. *The Lancet Neurology* **2024**, *23*, 669.

(10) Matsui, H.; Ito, S.; Matsui, H.; Ito, J.; Gabdulkhaev, R.; Hirose, M.; Yamanaka, T.; Koyama, A.; Kato, T.; Tanaka, M. *et al.* Phosphorylation of α-synuclein at T64 results in distinct oligomers and exerts toxicity in models of Parkinson's disease. *Proceedings of the National Academy of Sciences* **2023**, *120*, e2214652120.

(11) Fujiwara, H.; Hasegawa, M.; Dohmae, N.; Kawashima, A.; Masliah, E.; Goldberg, M. S.; Shen, J.; Takio, K.; Iwatsubo, T. α-Synuclein Is Phosphorylated in Synucleinopathy Lesions. *Nature Cell Biology* **2002**, *4*, 160–164.

(12) Ramalingam, N.; Jin, S.-X.; Moors, T. E.; Fonseca-Ornelas, L.; Shimanaka, K.; Lei, S.; Cam, H. P.; Watson, A. H.; Brontesi, L.; Ding, L. *et al.* Dynamic Physiological α-

synuclein S129 Phosphorylation Is Driven By Neuronal Activity. *npj Parkinson's Disease* **2023**, *9*, 4.

(13) Ramalingam, N.; Haass, C.; Dettmer, U. Physiological Roles of α-synuclein Serine-129 Phosphorylation - Not an Oxymoron. *Trends in Neurosciences* **2024**, *nil*, nil.

(14) Ghanem, S. S.; Majbour, N. K.; Vaikath, N. N.; Ardah, M. T.; Erskine, D.; Jensen, N. M.; Fayyad, M.; Sudhakaran, I. P.; Vasili, E.; Melachroinou, K. *et al.* α-Synuclein phosphorylation at serine 129 occurs after initial protein deposition and inhibits seeded fibril formation and toxicity. *Proceedings of the National Academy of Sciences* **2022**, *119*, e2109617119.

(15) Wang, Y.; Shi, M.; Chung, K. A.; Zabetian, C. P.; Leverenz, J. B.; Berg, D.; Srulijes, K.; Trojanowski, J. Q.; Lee, V. M.-Y.; Siderowf, A. D. *et al.* Phosphorylated α-synuclein in Parkinson's disease. *Science translational medicine* **2012**, *4*, 121ra20–121ra20.

(16) Kawahata, I.; Finkelstein, D. I.; Fukunaga, K. Pathogenic Impact of α-Synuclein Phosphorylation and Its Kinases in α-Synucleinopathies. *International Journal of Molecular Sciences* **2022**, *23*, 6216.

(17) Oueslati, A.; Fournier, M.; Lashuel, H. A. Role of post-translational modifications in modulating the structure, function and toxicity of α-synuclein: implications for Parkinson's disease pathogenesis and therapies. *Progress in brain research* **2010**, *183*, 115–145.

(18) Fauvet, B.; Fares, M.-B.; Samuel, F.; Dikiy, I.; Tandon, A.; Eliezer, D.; Lashuel, H. A. Characterization of Semisynthetic and Naturally Nα-Acetylated α-Synuclein in Vitro and in Intact Cells. *Journal of Biological Chemistry* **2012**, *287*, 28243–28262.

(19) Xie, Y.; Jiang, Y.; Ben-Amotz, D. Detection of amino acid and peptide phosphate protonation using Raman spectroscopy. *Analytical biochemistry* **2005**, *343*, 223–230.

(20) Schreurs, S.; Gerard, M.; Derua, R.; Waelkens, E.; Taymans, J.-M.; Baekelandt, V.; Engelborghs, Y. In vitro phosphorylation does not influence the aggregation kinetics of WT α-synuclein in contrast to its phosphorylation mutants. *International journal of molecular sciences* **2014**, *15*, 1040–1067.

(21) Samuel, F.; Flavin, W. P.; Iqbal, S.; Pacelli, C.; Renganathan, S. D. S.; Trudeau, L.-E.; Campbell, E. M.; Fraser, P. E.; Tandon, A. Effects of serine 129 phosphorylation on α-synuclein aggregation, membrane association, and internalization. *Journal of Biological Chemistry* **2016**, *291*, 4374–4385.

(22) Paleologou, K. E.; Schmid, A. W.; Rospigliosi, C. C.; Kim, H.-Y.; Lamberto, G. R.; Fredenburg, R. A.; Lansbury, P. T.; Fernandez, C. O.; Eliezer, D.; Zweckstetter, M. *et al.* Phosphorylation at Ser-129 but not the phosphomimics S129E/D inhibits the fibrillation of α-synuclein. *Journal of Biological Chemistry* **2008**, *283*, 16895–16905.

(23) Huang, J.; Rauscher, S.; Nawrocki, G.; Ran, T.; Feig, M.; de Groot, B. L.; Grubmüller, H.; MacKerell, A. D. Charmm36m: an Improved Force Field for Folded and Intrinsically Disordered Proteins. *Nature Methods* **2016**, *14*, 71–73.

(24) Semenyuk, P. I. Alpha-Synuclein Phosphorylation Induces Amyloid Conversion Via Enhanced Electrostatic Bridging: Insights From Molecular Modeling of the Full-Length Protein. *Biophysical Chemistry* **2024**, *307*, 107196.

(25) Kang, L.; Moriarty, G. M.; Woods, L. A.; Ashcroft, A. E.; Radford, S. E.; Baum, J. N-Terminal Acetylation of α-synuclein Induces Increased Transient Helical Propensity and Decreased Aggregation Rates in the Intrinsically Disordered Monomer. *Protein Science* **2012**, *21*, 911–917.

(26) Trexler, A. J.; Rhoades, E. N-terminal Acetylation Is Critical for Forming α-helical Oligomer of α-synuclein. *Protein Science* **2012**, *21*, 601–605.

(27) Maltsev, A. S.; Ying, J.; Bax, A. Impact of N-terminal acetylation of α-synuclein on its random coil and lipid binding properties. *Biochemistry* **2012**, *51*, 5004–5013.

(28) Piana, S.; Robustelli, P.; Tan, D.; Chen, S.; Shaw, D. E. Development of a force field for the simulation of single-chain proteins and protein–protein complexes. *Journal of chemical theory and computation* **2020**, *16*, 2494–2507.

(29) Robustelli, P.; Piana, S.; Shaw, D. E. Developing a molecular dynamics force field for both folded and disordered protein states. *Proceedings of the National Academy of Sciences* **2018**, *115*, E4758–E4766.

(30) Wang, W. Recent advances in atomic molecular dynamics simulation of intrinsically disordered proteins. *Phys. Chem. Chem. Phys.* **2021**, *23*, 777–784.

(31) Pedersen, K. B.; Flores-Canales, J. C.; Schiøtt, B. Predicting molecular properties of α-synuclein using force fields for intrinsically disordered proteins. *Proteins: Structure, Function, and Bioinformatics* **2023**, *91*, 47–61.

(32) Robustelli, P.; de Opakua, A. I.; Campbell-Bezat, C.; Giordanetto, F.; Becker, S.; Zweckstetter, M.; Pan, A. C.; Shaw, D. E. Molecular Basis of Small-Molecule Binding To α-Synuclein. *Journal of the American Chemical Society* **2022**, *144*, 2501–2510.

(33) Homeyer, N.; Horn, A. H.; Lanig, H.; Sticht, H. AMBER force-field parameters for phosphorylated amino acids in different protonation states: phosphoserine, phosphothreonine, phosphotyrosine, and phosphohistidine. *Journal of molecular modeling* **2006**, *12*, 281–289.

(34) Steinbrecher, T.; Latzer, J.; Case, D. Revised AMBER parameters for bioorganic phosphates. *Journal of chemical theory and computation* **2012**, *8*, 4405–4412.

(35) Khoury, G. A.; Thompson, J. P.; Smadbeck, J.; Kieslich, C. A.; Floudas, C. A. Forcefield_PTM: Ab initio charge and AMBER forcefield parameters for frequently oc-

curring post-translational modifications. *Journal of chemical theory and computation* **2013**, *9*, 5653–5674.

(36) Petrov, D.; Margreitter, C.; Grandits, M.; Oostenbrink, C.; Zagrovic, B. A systematic framework for molecular dynamics simulations of protein post-translational modifications. *PLoS computational biology* **2013**, *9*, e1003154.

(37) Zhong, B.; Song, G.; Chen, H.-F. Balanced Force Field ff03CMAP Improving the Dynamics Conformation Sampling of Phosphorylation Site. *International Journal of Molecular Sciences* **2022**, *23*, 11285.

(38) Vymětal, J.; Jurásková, V.; Vondrášek, J. AMBER and CHARMM force fields inconsistently portray the microscopic details of phosphorylation. *Journal of Chemical Theory and Computation* **2018**, *15*, 665–679.

(39) Rieloff, E.; Skepö, M. Phosphorylation of a disordered peptide—Structural effects and force field inconsistencies. *Journal of chemical theory and computation* **2020**, *16*, 1924–1935.

(40) Rieloff, E.; Skepö, M. Molecular Dynamics Simulations of Phosphorylated Intrinsically Disordered Proteins: a Force Field Comparison. *International Journal of Molecular Sciences* **2021**, *22*, 10174.

(41) Man, V. H.; He, X.; Gao, J.; Wang, J. Phosphorylation of Tau R2 Repeat Destabilizes Its Binding to Microtubules: A Molecular Dynamics Simulation Study. *ACS Chemical Neuroscience* **2023**,

(42) Tucker, M. R.; Piana, S.; Tan, D.; LeVine, M. V.; Shaw, D. E. Development of Force Field Parameters for the Simulation of Single- and Double-Stranded Dna Molecules and Dna-Protein Complexes. *The Journal of Physical Chemistry B* **2022**, *126*, 4442–4457.

(43) Irbäck, A.; Mohanty, S. Profasi: a Monte Carlo Simulation Package for Protein Folding and Aggregation. *Journal of Computational Chemistry* **2006**, *27*, 1548–1555.

(44) D'Urzo, A.; Konijnenberg, A.; Rossetti, G.; Habchi, J.; Li, J.; Carloni, P.; Sobott, F.; Longhi, S.; Grandori, R. Molecular Basis for Structural Heterogeneity of an Intrinsically Disordered Protein Bound To a Partner By Combined Esi-Im-Ms and Modeling. *Journal of The American Society for Mass Spectrometry* **2014**, *26*, 472–481.

(45) Cragnell, C.; Rieloff, E.; Skepö, M. Utilizing Coarse-Grained Modeling and Monte Carlo Simulations To Evaluate the Conformational Ensemble of Intrinsically Disordered Proteins and Regions. *Journal of Molecular Biology* **2018**, *430*, 2478–2492.

(46) Rieloff, E.; Tully, M. D.; Skepö, M. Assessing the Intricate Balance of Intermolecular Interactions Upon Self-Association of Intrinsically Disordered Proteins. *Journal of Molecular Biology* **2019**, *431*, 511–523.

(47) Shrestha, U. R.; Smith, J. C.; Petridis, L. Full Structural Ensembles of Intrinsically Disordered Proteins From Unbiased Molecular Dynamics Simulations. *Communications Biology* **2021**, *4*, 243.

(48) Gupta, A.; Dey, S.; Hicks, A.; Zhou, H.-X. Artificial Intelligence Guided Conformational Mining of Intrinsically Disordered Proteins. *Communications Biology* **2022**, *5*, 610.

(49) Yu, H.; Han, W.; Ma, W.; Schulten, K. Transient β-hairpin Formation in α-synuclein Monomer Revealed By Coarse-Grained Molecular Dynamics Simulation. *The Journal of Chemical Physics* **2015**, *143*, 243142.

(50) Cragnell, C.; Durand, D.; Cabane, B.; Skepö, M. Coarse-Grained Modeling of the Intrinsically Disordered Protein Histatin 5 in Solution: Monte Carlo Simulations in Combination With Saxs. *Proteins: Structure, Function, and Bioinformatics* **2016**, *84*, 777–791.

(51) Hyltegren, K.; Polimeni, M.; Skepö, M.; Lund, M. Integrating All-Atom and Coarse-Grained Simulations-Toward Understanding of Idps At Surfaces. *Journal of Chemical Theory and Computation* **2020**, *16*, 1843–1853.

(52) Garaizar, A.; Espinosa, J. R. Salt Dependent Phase Behavior of Intrinsically Disordered Proteins From a Coarse-Grained Model With Explicit Water and Ions. *The Journal of Chemical Physics* **2021**, *155*, 125103.

(53) Wang, L.; Friesner, R. A.; Berne, B. Replica exchange with solute scaling: a more efficient version of replica exchange with solute tempering (REST2). *The Journal of Physical Chemistry B* **2011**, *115*, 9431–9438.

(54) Rossetti, G.; Musiani, F.; Abad, E.; Dibenedetto, D.; Mouhib, H.; Fernandez, C. O.; Carloni, P. Conformational ensemble of human α-synuclein physiological form predicted by molecular simulations. *Physical Chemistry Chemical Physics* **2016**, *18*, 5702–5706.

(55) Palomino-Hernandez, O.; Buratti, F. A.; Sacco, P. S.; Rossetti, G.; Carloni, P.; Fernandez, C. O. Role of Tyr-39 for the Structural Features of α-Synuclein and for the Interaction with a Strong Modulator of Its Amyloid Assembly. *International journal of molecular sciences* **2020**, *21*, 5061.

(56) Theillet, F.-X.; Binolfi, A.; Bekei, B.; Martorana, A.; Rose, H. M.; Stuiver, M.; Verzini, S.; Lorenz, D.; Van Rossum, M.; Goldfarb, D. *et al.* Structural disorder of monomeric α-synuclein persists in mammalian cells. *Nature* **2016**, *530*, 45–50.

(57) Uluca, B.; Viennet, T.; Petrović, D.; Shaykhalishahi, H.; Weirich, F.; Gönülalan, A.; Strodel, B.; Etzkorn, M.; Hoyer, W.; Heise, H. DNP-enhanced MAS NMR: a tool to snapshot conformational ensembles of α-synuclein in different states. *Biophysical journal* **2018**, *114*, 1614–1623.

(58) Jain, K.; Ghribi, O.; Delhommelle, J. Folding free-energy landscape of α-synuclein (35–97) via replica exchange molecular dynamics. *Journal of Chemical Information and Modeling* **2020**, *61*, 432–443.

(59) Ilie, I. M.; Nayar, D.; Den Otter, W. K.; Van Der Vegt, N. F.; Briels, W. J. Intrinsic conformational preferences and interactions in α-synuclein fibrils: insights from molecular dynamics simulations. *Journal of chemical theory and computation* **2018**, *14*, 3298–3310.

(60) Chwastyk, M.; Cieplak, M. Conformational biases of α-synuclein and formation of transient knots. *The Journal of Physical Chemistry B* **2019**, *124*, 11–19.

(61) Perlmutter, J. D.; Braun, A. R.; Sachs, J. N. Curvature dynamics of α-synuclein familial parkinson disease mutants. *Journal of Biological Chemistry* **2009**, *284*, 7177–7189.

(62) Allison, J. R.; Varnai, P.; Dobson, C. M.; Vendruscolo, M. Determination of the free energy landscape of α-synuclein using spin label nuclear magnetic resonance measurements. *Journal of the American Chemical Society* **2009**, *131*, 18314–18326.

(63) Amos, S.-B. T.; Schwarz, T. C.; Shi, J.; Cossins, B. P.; Baker, T. S.; Taylor, R. J.; Konrat, R.; Sansom, M. S. Membrane Interactions of α-Synuclein Revealed by Multiscale Molecular Dynamics Simulations, Markov State Models, and NMR. *The Journal of Physical Chemistry B* **2021**, *125*, 2929–2941.

(64) Herrera, F. E.; Chesi, A.; Paleologou, K. E.; Schmid, A.; Munoz, A.; Vendruscolo, M.; Gustincich, S.; Lashuel, H. A.; Carloni, P. Inhibition of α-synuclein fibrillization by dopamine is mediated by interactions with five C-terminal residues and with E83 in the NAC region. *PloS one* **2008**, *3*, e3394.

(65) Robustelli, P.; Ibanez-de Opakua, A.; Campbell-Bezat, C.; Giordanetto, F.; Becker, S.;

Zweckstetter, M.; Pan, A. C.; Shaw, D. E. Molecular basis of small-molecule binding to α-synuclein. *Journal of the American Chemical Society* **2022**, *144*, 2501–2510.

(66) Balesh, D.; Ramjan, Z., *et al.* Unfolded annealing molecular dynamics conformers for wild-type and disease-associated variants of alpha-synuclein show no propensity for beta-sheetformation. *Journal of Biophysical Chemistry* **2011**, *2011*.

(67) Allison, J. R.; Rivers, R. C.; Christodoulou, J. C.; Vendruscolo, M.; Dobson, C. M. A relationship between the transient structure in the monomeric state and the aggregation propensities of α-synuclein and β-synuclein. *Biochemistry* **2014**, *53*, 7170–7183.

(68) Dedmon, M. M.; Lindorff-Larsen, K.; Christodoulou, J.; Vendruscolo, M.; Dobson, C. M. Mapping long-range interactions in α-synuclein using spin-label NMR and ensemble molecular dynamics simulations. *Journal of the American Chemical Society* **2005**, *127*, 476–477.

(69) Park, S.; Yoon, J.; Jang, S.; Lee, K.; Shin, S. The role of the acidic domain of α-synuclein in amyloid fibril formation: a molecular dynamics study. *Journal of Biomolecular Structure and Dynamics* **2016**, *34*, 376–383.

(70) Brodie, N. I.; Popov, K. I.; Petrotchenko, E. V.; Dokholyan, N. V.; Borchers, C. H. Conformational ensemble of native α-synuclein in solution as determined by short-distance crosslinking constraint-guided discrete molecular dynamics simulations. *PLoS computational biology* **2019**, *15*, e1006859.

(71) Tsigelny, I. F.; Bar-On, P.; Sharikov, Y.; Crews, L.; Hashimoto, M.; Miller, M. A.; Keller, S. H.; Platoshyn, O.; Yuan, J. X.-J.; Masliah, E. Dynamics of α-synuclein aggregation and inhibition of pore-like oligomer development by β-synuclein. *The FEBS journal* **2007**, *274*, 1862–1877.

(72) Ramis, R.; Ortega-Castro, J.; Casasnovas, R.; Mariño, L.; Vilanova, B.; Adrover, M.; Frau, J. A coarse-grained molecular dynamics approach to the study of the intrinsically

disordered protein α-synuclein. *Journal of chemical information and modeling* **2019**, *59*, 1458–1471.

(73) Yu, H.; Han, W.; Ma, W.; Schulten, K. Transient β-hairpin formation in α-synuclein monomer revealed by coarse-grained molecular dynamics simulation. *The Journal of chemical physics* **2015**, *143*, 12B623_1.

(74) Narayanan, C.; Weinstock, D. S.; Wu, K.-P.; Baum, J.; Levy, R. M. Investigation of the polymeric properties of α-synuclein and comparison with NMR experiments: a replica exchange molecular dynamics study. *Journal of chemical theory and computation* **2012**, *8*, 3929–3942.

(75) Dibenedetto, D.; Rossetti, G.; Caliandro, R.; Carloni, P. A molecular dynamics simulation-based interpretation of nuclear magnetic resonance multidimensional heteronuclear spectra of α-synuclein· dopamine adducts. *Biochemistry* **2013**, *52*, 6672–6683.

(76) Tsigelny, I. F.; Sharikov, Y.; Miller, M. A.; Masliah, E. Mechanism of alpha-synuclein oligomerization and membrane interaction: theoretical approach to unstructured proteins studies. *Nanomedicine: Nanotechnology, Biology and Medicine* **2008**, *4*, 350–357.

(77) Zhang, T.; Tian, Y.; Li, Z.; Liu, S.; Hu, X.; Yang, Z.; Ling, X.; Liu, S.; Zhang, J. Molecular dynamics study to investigate the dimeric structure of the full-length α-synuclein in aqueous solution. *Journal of Chemical Information and Modeling* **2017**, *57*, 2281–2293.

(78) Savva, L.; Platts, J. A. How Cu (II) binding affects structure and dynamics of α-synuclein revealed by molecular dynamics simulations. *Journal of Inorganic Biochemistry* **2023**, *239*, 112068.

(79) Razzokov, J.; Fazliev, S.; Makhkamov, M.; Marimuthu, P.; Baev, A.; Kurganov, E.

Effect of Electric Field on α-Synuclein Fibrils: Revealed by Molecular Dynamics Simulations. *International Journal of Molecular Sciences* **2023**, *24*, 6312.

(80) Savva, L.; Platts, J. A. Exploring the Impact of Mutation and Post-Translational Modification on α-Synuclein: Insights From Molecular Dynamics Simulations With and Without Copper. *Journal of Inorganic Biochemistry* **2023**, *249*, 112395.

(81) Jin, F.; Gräter, F. How Multisite Phosphorylation Impacts the Conformations of Intrinsically Disordered Proteins. *PLOS Computational Biology* **2021**, *17*, e1008939.

(82) Rieloff, E.; Skepö, M. The Effect of Multisite Phosphorylation on the Conformational Properties of Intrinsically Disordered Proteins. *International Journal of Molecular Sciences* **2021**, *22*, 11058.

(83) Martin, I. M.; Aponte-Santamaría, C.; Schmidt, L.; Hedtfeld, M.; Iusupov, A.; Musacchio, A.; Gräter, F. Phosphorylation Tunes Elongation Propensity and Cohesiveness of Incenp's Intrinsically Disordered Region. *Journal of Molecular Biology* **2022**, *434*, 167387.

(84) Adhikari, S.; Mondal, J. Machine Learning Subtle Conformational Change Due To Phosphorylation in Intrinsically Disordered Proteins. *The Journal of Physical Chemistry B* **2023**, *127*, 9433–9449.

(85) Amith, W. D.; Dutagaci, B. Complex Conformational Space of the Rna Polymerase Ii C-Terminal Domain Upon Phosphorylation. *The Journal of Physical Chemistry B* **2023**, *127*, 9223–9235.

(86) Roche, J.; Ying, J.; Maltsev, A. S.; Bax, A. Impact of Hydrostatic Pressure on an Intrinsically Disordered Protein: A High-Pressure NMR Study of α-Synuclein. *ChemBioChem* **2013**, *14*, 1754–1761.

(87) DeLano, W. L. Pymol: An open-source molecular graphics tool. *CCP4 Newsletter on protein crystallography* **2002**, *40*, 82–92.

(88) Piana, S.; Donchev, A. G.; Robustelli, P.; Shaw, D. E. Water Dispersion Interactions Strongly Influence Simulated Structural Properties of Disordered Protein States. *The Journal of Physical Chemistry B* **2015**, *119*, 5113–5123.

(89) Darden, T.; York, D.; Pedersen, L. Particle mesh Ewald: An N log (N) method for Ewald sums in large systems. *The Journal of chemical physics* **1993**, *98*, 10089–10092.

(90) Evans, D. J.; Holian, B. L. The nose–hoover thermostat. *The Journal of chemical physics* **1985**, *83*, 4069–4074.

(91) Andersen, H. C. Molecular dynamics simulations at constant pressure and/or temperature. *The Journal of chemical physics* **1980**, *72*, 2384–2393.

(92) Hess, B.; Bekker, H.; Berendsen, H. J.; Fraaije, J. G. LINCS: a linear constraint solver for molecular simulations. *Journal of computational chemistry* **1997**, *18*, 1463–1472.

(93) Appadurai, R.; Koneru, J. K.; Bonomi, M.; Robustelli, P.; Srivastava, A. Clustering Heterogeneous Conformational Ensembles of Intrinsically Disordered Proteins With T-Distributed Stochastic Neighbor Embedding. *Journal of Chemical Theory and Computation* **2023**, *19*, 4711–4727.

(94) McGibbon, R. T.; Beauchamp, K. A.; Harrigan, M. P.; Klein, C.; Swails, J. M.; Hernández, C. X.; Schwantes, C. R.; Wang, L.-P.; Lane, T. J.; Pande, V. S. MDTraj: A Modern Open Library for the Analysis of Molecular Dynamics Trajectories. *Biophysical Journal* **2015**, *109*, 1528 – 1532.

(95) Shen, Y.; Bax, A. Sparta+: a Modest Improvement in Empirical Nmr Chemical Shift Prediction By Means of an Artificial Neural Network. *Journal of Biomolecular NMR* **2010**, *48*, 13–22.

(96) Nagy, G.; Igaev, M.; Jones, N. C.; Hoffmann, S. V.; Grubmüller, H. Sesca: Predicting Circular Dichroism Spectra From Protein Molecular Structures. *Journal of Chemical Theory and Computation* **2019**, *15*, 5087–5102.

(97) Nagy, G.; Grubmüller, H. How Accurate Is Circular Dichroism-Based Model Validation? *European Biophysics Journal* **2020**, *49*, 497–510.

(98) Nagy, G.; Grubmuller, H. Implementation of a Bayesian Secondary Structure Estimation Method for the Sesca Circular Dichroism Analysis Package. *Computer Physics Communications* **2021**, *266*, 108022.

(99) de Bruyn, E. SPEADI: Scalable Protein Environment Analysis for Dynamics and Ions (v1.0.0). 2022; `https://doi.org/10.5281/zenodo.7436713`.

(100) de Bruyn, E.; Dorn, A. E.; Zimmermann, O.; Rossetti, G. Speadi: Accelerated Analysis of Idp-Ion Interactions From MD-Trajectories. *Biology* **2023**, *12*, 581.

(101) Wernet, P.; Nordlund, D.; Bergmann, U.; Cavalleri, M.; Odelius, M.; Ogasawara, H.; Näslund, L. A.; Hirsch, T. K.; Ojamäe, L.; Glatzel, P. *et al.* The Structure of the First Coordination Shell in Liquid Water. *Science* **2004**, *304*, 995–999.

(102) Donald, J. E.; Kulp, D. W.; DeGrado, W. F. Salt Bridges: Geometrically Specific, Designable Interactions. *Proteins: Structure, Function, and Bioinformatics* **2011**, *79*, 898–915.

(103) Kabsch, W.; Sander, C. Dictionary of protein secondary structure: pattern recognition of hydrogen-bonded and geometrical features. *Biopolymers: Original Research on Biomolecules* **1983**, *22*, 2577–2637.

(104) Tavernelli, I.; Cotesta, S.; Iorio, E. E. D. Protein Dynamics, Thermal Stability, and Free-Energy Landscapes: a Molecular Dynamics Investigation. *Biophysical Journal* **2003**, *85*, 2641–2649.

(105) Lazar, T.; Guharoy, M.; Vranken, W.; Rauscher, S.; Wodak, S. J.; Tompa, P. Distance-Based metrics for comparing conformational ensembles of intrinsically disordered proteins. *Biophysical Journal* **2020**, *118*, 2952–2965.

(106) Li, J.; Bennett, K. C.; Liu, Y.; Martin, M. V.; Head-Gordon, T. Accurate Prediction of Chemical Shifts for Aqueous Protein Structure on "Real World" Data. *Chemical Science* **2020**, *11*, 3180–3191.

(107) Bell, R.; Vendruscolo, M. Modulation of the Interactions Between α-Synuclein and Lipid Membranes By Post-Translational Modifications. *Frontiers in Neurology* **2021**, *12*, nil.

(108) Killinger, B. A.; Mercado, G.; Choi, S.; Tittle, T.; Chu, Y.; Brundin, P.; Kordower, J. H. Distribution of Phosphorylated Alpha-Synuclein in Non-Diseased Brain Implicates Olfactory Bulb Mitral Cells in Synucleinopathy Pathogenesis. *npj Parkinson's Disease* **2023**, *9*, 43.

(109) Guerrero-Ferreira, R.; Taylor, N. M.; Mona, D.; Ringler, P.; Lauer, M. E.; Riek, R.; Britschgi, M.; Stahlberg, H. Cryo-Em Structure of Alpha-Synuclein Fibrils. *eLife* **2018**, *7*, nil.

(110) Guerrero-Ferreira, R.; Taylor, N. M.; Arteni, A.-A.; Kumari, P.; Mona, D.; Ringler, P.; Britschgi, M.; Lauer, M. E.; Makky, A.; Verasdonck, J. *et al.* Two New Polymorphic Structures of Human Full-Length Alpha-Synuclein Fibrils Solved By Cryo-Electron Microscopy. *eLife* **2019**, *8*, nil.

(111) Krause, D. Juwels: Modular Tier-0/1 Supercomputer At Jülich Supercomputing Centre. *Journal of large-scale research facilities JLSRF* **2019**, *5*, A135.

(112) Alvarez, D. Juwels Cluster and Booster: Exascale Pathfinder With Modular Supercomputing Architecture At Juelich Supercomputing Centre. *Journal of large-scale research facilities JLSRF* **2021**, *7*, A183.

(113) Herten, A. JUWELS Booster - Early User Experiences. Proceedings of the 2021 on Performance EngineeRing, Modelling, Analysis, and VisualizatiOn STrategy. 2021; p nil.

(114) Kesselheim, S.; Herten, A.; Krajsek, K.; Ebert, J.; Jitsev, J.; Cherti, M.; Langguth, M.; Gong, B.; Stadtler, S.; Mozaffari, A. *et al. Lecture Notes in Computer Science*; Lecture Notes in Computer Science; Springer International Publishing, 2021; pp 453–468.

(115) Thörnig, P. Jureca: Data Centric and Booster Modules Implementing the Modular Supercomputing Architecture At Jülich Supercomputing Centre. *Journal of large-scale research facilities JLSRF* **2021**, *7*, A182.

TOC Graphic

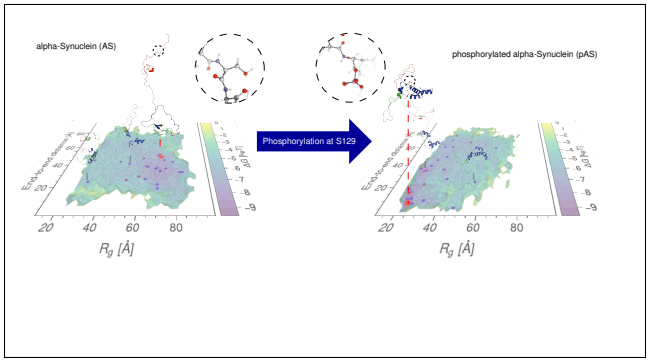
alpha-Synuclein (AS)
phosphorylated alpha-Synuclein (pAS)
Phosphorylation at S129
20
40
60
80
R_g [Å]